

1 Word Count: 2426

Revision 1

2

3 **Element loss to platinum capsules in high-temperature–pressure experiments**

4 Jintuan Wang<sup>1,\*</sup>, Xiaolin Xiong<sup>1,\*</sup>, Le Zhang<sup>1</sup>, and Eiichi Takahashi<sup>1</sup>

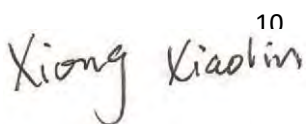
5

6 1 State Key Laboratory of Isotope Geochemistry, Guangzhou Institute of Geochemistry,

7 CAS, Guangzhou 510640, China

8

9 

10 

12 

13 

14

15

16

## ABSTRACT

17 Element partition coefficients play key roles in understanding various geological  
18 processes and are typically measured by performing high-temperature–pressure (HTP)  
19 experiments. In HTP experiments, samples are usually enclosed in capsules made of  
20 noble metals. Previous studies have shown that Fe, Ni, and Cu readily alloy with noble  
21 metals, resulting in significant loss of these elements from the experimental samples. The  
22 loss of elements could severely undermine phase equilibrium, and compromise the  
23 validity and accuracy of the obtained partition coefficients. However, it remains unclear if  
24 other elements (in addition to Fe, Ni, and Cu) will also be lost from samples during HTP  
25 experiments, and how to minimize such losses. We performed a series of experiments at 1  
26 GPa and 1400 °C to investigate which element will be lost from samples and explore the  
27 influence of capsule materials and oxygen fugacity ( $fO_2$ ) on the loss behavior of elements.  
28 The starting material is a synthesized basaltic glass consisting of 8 major elements and 37  
29 trace elements. The sample capsules included platinum (Pt), graphite-lined Pt, and  
30 rhenium-lined Pt, and the experimental oxygen fugacity ( $fO_2$ ) was buffered from <FMQ–  
31 2 to ~FMQ+5. Results show that: (1) 15 elements (V, Cr, Mn, Fe, Co, Ni, Cu, Zn, Ga, Ge,  
32 Cd, In, Sn, W, and Mo) were lost from the sample due to direct contacting and alloying  
33 with Pt under graphite-buffered conditions; (2) graphite- and Re-lined lining can  
34 physically isolate the starting material from Pt and prevent the loss of V, Cr, Mn, Fe, Zn,  
35 Ga, Ge, Cd, In, Sn, W, and Mo, but only slightly reduce the loss of Ni and Cu; and (3)  
36 element loss can be significantly reduced under oxidizing conditions, and all elements

37 except Cu were retained in the samples under Ru–RuO<sub>2</sub> buffered conditions. These  
38 findings provide several viable capsule assemblies that are capable of preventing or  
39 reducing element loss, which may prove useful in determining accurate partition  
40 coefficients in HTP experiments.

41 **Keywords:** element loss, high-temperature–pressure experiments, capsule materials,  
42 experimental  $fO_2$ .

43

44

## INTRODUCTION

45 The partitioning behavior of elements is critical to our understanding of various  
46 geological processes, including partial melting of rocks in the mantle and crust (Foley et  
47 al., 2002; Matzen et al., 2013, 2017; Rapp et al., 2003; Sobolev et al., 2005, 2007; Xiong  
48 et al., 2005, 2006, 2011), fractional crystallization of magmas (Davidson et al., 2007; Lee  
49 and Tang, 2020; Li et al., 2017), ore formation in magmatic–hydrothermal systems (Liu  
50 et al., 2015; Zajacz et al., 2011, 2012, 2017), and redox state of magmas and their sources  
51 (Canil, 1997; Lee et al., 2005; Wang et al., 2019). Element partition coefficients between  
52 mineral and melt (D values) are typically obtained using two approaches. The first is the  
53 phenocryst–matrix method, in which partition coefficients are determined by analyzing  
54 the elemental concentrations of phenocrysts and coexisting matrix in natural volcanic  
55 rocks (Philpotts and Schnetzler, 1970; Portnyagin et al., 2017; Schnetzler and Philpotts,  
56 1970). However, the accuracy of the phenocryst–matrix method is influenced by various  
57 factors, such as disequilibrium between the phenocrysts and matrix, as well as

58 uncertainties in temperature, pressure, and  $fO_2$  conditions. The second approach is HTP  
59 experiments, in which coexisting minerals and melt are synthesized at HTP conditions. In  
60 a HTP experiment, the temperature, pressure, and  $fO_2$  are well controlled, and chemical  
61 equilibrium can be approached by extending the duration of the experiments. Thus, HTP  
62 experiments have been widely used to determine mineral/melt D values. In HTP  
63 experiments, samples are usually enclosed in capsules made of noble metals. However, a  
64 notorious problem in such experiments is that certain elements, including Fe, Ni, and Cu,  
65 are lost from the experimental samples by alloying with the noble metal capsules (Adam  
66 and Green, 2006; Filiberto et al., 2009; Grove, 1981; Merrill and Wyllie, 1973; Ratajeski  
67 and Sisson, 1999). Although Au and Au–Pd capsules suffer less element loss, these  
68 materials are only applicable at relatively low temperatures (Kawamoto and Hirose, 1994;  
69 Ratajeski and Sisson, 1999). Element loss in HTP experiments can severely undermine  
70 phase equilibrium and compromise the validity and accuracy of measured D values  
71 (Adam and Green, 2006; Fellows and Canil, 2012; Liu et al., 2014, 2015; Zajacz et al.,  
72 2011, 2012). Though the “pre-saturation” technique works well in minimizing iron loss in  
73 Pt (Grove, 1981) and copper loss in Au (Zajacz et al., 2011), it remains unclear if other  
74 elements (in addition to Fe, Ni, and Cu) will also be lost from experimental samples, and  
75 how to prevent or minimize such loss. Here, we investigate the loss behavior of 45  
76 elements in Pt capsule at 1400 °C and 1 GPa, and explore the effects of capsule materials  
77 and experimental  $fO_2$  on it. Based on the results, we propose new capsule assemblies that  
78 minimize element loss from samples during HTP experiments.

79

80

## EXPERIMENTAL AND ANALYTICAL METHODS

### 81 **High-temperature–pressure experiments**

82 A synthesized high-Mg basalt (HMB) was used as the starting material. The HMB  
83 glass is composed of 8 major elements (SiO<sub>2</sub>, TiO<sub>2</sub>, Al<sub>2</sub>O<sub>3</sub>, FeO, MgO, CaO, Na<sub>2</sub>O, and  
84 K<sub>2</sub>O) and 37 trace elements, including large-ion lithophile elements (Li, B, Rb, Sr, Ba,  
85 and Cs), rare earth elements (La, Ce, Pr, Nd, Sm, Eu, Gd, Ho, Yb, Lu, and Y),  
86 high-field-strength elements (Zr, Hf, Nb, Ta, P, Sn, W, and Mo), transition elements (Sc, V,  
87 Cr, Mn, Co, Ni, Cu, and Zn), and metalloid elements (Ga, Ge, Cd, and In). The major and  
88 trace element composition of the HMB glass is homogeneous (Supplementary Table 1).  
89 Details of the synthesizing procedures are described in Wang et al. (2019). The trace  
90 element contents range between 15 and 1700 ppm, with most contents being ~70 ppm  
91 (Supplementary Table 1).

92 All of the experiments were conducted at 1 GPa and 1400 °C using a Rockland  
93 piston–cylinder apparatus at Guangzhou Institute of Geochemistry, Chinese Academy of  
94 Sciences. We used a half-inch assembly that comprises a talc sleeve, pyrex glass, graphite  
95 furnace, MgO inserts, and sample capsule. The experimental temperature was controlled  
96 using a Eurotherm controller and monitored with a Pt–Pt<sub>90</sub>Rh<sub>10</sub> thermocouple (S-type). A  
97 friction correction of –13% was applied to the apparatus (Liu et al., 2015). The pressure  
98 uncertainty in the experiments was about 0.1 GPa, and the temperature gradient along the  
99 sample capsule was <15 °C. For each experiment, the HMB powder was sealed into

100 platinum (Pt) capsules (3.0 mm outer diameter; 2.7 mm inner diameter; 6 mm length)  
101 together with 0.8 to 3.7 wt.% H<sub>2</sub>O. Within the capsules, different sample assemblies and  
102 *f*O<sub>2</sub> buffers (Fig. 1) were used to change the capsule materials and buffer the experimental  
103 *f*O<sub>2</sub>. The experiments were terminated by turning off the power to the heater. The  
104 recovered run products were sectioned, mounted in epoxy resin, and polished. Reflected  
105 light microscopy and back-scattered electron images show that all of the samples  
106 quenched to clear glass (Fig. 1), indicating that the samples were melts during the  
107 experiments.

108

#### 109 **LA-ICP-MS analysis**

110 Trace element concentrations in the starting HMB glass and quenched glasses were  
111 analyzed using an ELEMENT XR (Thermo Fisher Scientific) ICP-MS coupled with a  
112 193 nm Resolution M-50 (Resonetics) laser ablation system at Guangzhou Institute of  
113 Geochemistry. Laser ablation was performed with an energy density of 4 J/cm<sup>2</sup>, a  
114 repetition rate of 5 Hz, and a spot size of 33 μm. For each analysis, the gas blank and  
115 sample signal were collected for 20 and 30 s, respectively. Signals of the following  
116 isotopes were detected: <sup>7</sup>Li, <sup>11</sup>B, <sup>23</sup>Na, <sup>25</sup>Mg, <sup>27</sup>Al, <sup>29</sup>Si, <sup>31</sup>P, <sup>39</sup>K, <sup>43</sup>Ca, <sup>45</sup>Sc, <sup>47</sup>Ti, <sup>51</sup>V, <sup>53</sup>Cr,  
117 <sup>55</sup>Mn, <sup>57</sup>Fe, <sup>59</sup>Co, <sup>60</sup>Ni, <sup>63</sup>Cu, <sup>66</sup>Zn, <sup>70</sup>Ge, <sup>71</sup>Ga, <sup>85</sup>Rb, <sup>88</sup>Sr, <sup>89</sup>Y, <sup>90</sup>Zr, <sup>93</sup>Nb, <sup>98</sup>Mo, <sup>111</sup>Cd, <sup>115</sup>In,  
118 <sup>118</sup>Sn, <sup>133</sup>Cs, <sup>137</sup>Ba, <sup>139</sup>La, <sup>140</sup>Ce, <sup>141</sup>Pr, <sup>146</sup>Nd, <sup>147</sup>Sm, <sup>151</sup>Eu, <sup>157</sup>Gd, <sup>165</sup>Ho, <sup>174</sup>Yb, <sup>175</sup>Lu,  
119 <sup>178</sup>Hf, <sup>181</sup>Ta, <sup>182</sup>W, and <sup>185</sup>Re. Reference materials GSD-1G, BHVO-2G, BCR-2G, NIST  
120 610, and NIST 612 were used as external standards, and the SiO<sub>2</sub> content (46.06 wt.%) of

121 the HMB glass was used as the internal standard. It is reasonable to use SiO<sub>2</sub> content as  
122 the internal standard because silica is inert under the experimental conditions used here,  
123 and also because we focus on element loss relative to the starting material. We also  
124 analyzed TB-1G (Elburg et al., 2005) as an unknown sample. The analytical precision (2 $\sigma$ )  
125 measured for TB-1G is better than  $\pm 10\%$  for all of the elements. Details of the analytical  
126 conditions and data processing procedures are described in Zhang et al. (2019).  
127 Analytical results are presented in Supplementary Table 1.

128

## 129 **EXPERIMENTAL RESULTS AND DISCUSSION**

### 130 **Time-series experiments**

131 Three experiments (using the capsule assembly shown in Fig. 1a) with different  
132 durations were conducted to investigate: (1) which elements will lose from the samples  
133 by alloying with the Pt capsule under reducing conditions; (2) how long it takes for the  
134 elements to reach equilibrium between metallic Pt and melt. These experiments were  
135 buffered by graphite at  $fO_2 < FMQ-2$  (Medard, 2008). As observed under a binocular  
136 stereo-microscope, the color of the quenched glasses varies systematically with  
137 experimental duration. The glass changed from dark green after 2 h (E1), to light green  
138 after 10 h (E2), and then to nearly transparent after 22 h (E3), suggesting a change in melt  
139 composition caused by continuous iron loss. The compositions of quenched glasses  
140 (normalized to the starting material) are shown in Fig. 2a. We found that 15 elements,  
141 including V, Cr, Mn, Fe, Co, Ni, Cu, Zn, Ga, Ge, Cd, In, Sn, W, and Mo, have lower

142 concentrations in the quenched glasses than in the HMB glass, indicating that they were  
143 lost from the samples. The concentrations of these 15 elements as a function of  
144 experimental duration are plotted in Fig. 2b. We found that element concentrations  
145 decreased markedly between 0 and 10 h, and then remained nearly constant from 10 to 22  
146 h, demonstrating that these 15 elements approached diffusional equilibrium within 10 h.  
147 All experiments described in the following sections were conducted for 22 h to ensure  
148 diffusional equilibrium.

149

### 150 **The effect of capsule materials**

151 Element loss in the experiments was mainly governed by experimental temperatures,  
152 capsule materials, and experimental  $fO_2$  values (O'Neill and Nell, 1997; Ratajeski and  
153 Sisson, 1999). Accordingly, it is possible to prevent element loss by changing the capsule  
154 materials or by elevating the experimental  $fO_2$ . To change the capsule materials, we lined  
155 the Pt capsules with graphite and rhenium (Re) foil. In the graphite-lined experiment (E4),  
156 the HMB powder was packed into a graphite capsule, which was then placed into the Pt  
157 capsule and welded shut (Fig. 1b). We noticed that a robust lining of the Pt capsule is  
158 crucial to avoid cracks on the graphite capsule. In the Re-lined experiment (E5), a Re  
159 tube and disks were used to insulate the HMB powder from the Pt capsule. We also  
160 inserted graphite disks at the bottom and top of the HMB powder to buffer the  
161 experimental  $fO_2$  (Fig. 1c). Including experiment E3, three samples (all buffered by  
162 graphite) encapsulated in a Pt capsule, graphite-lined Pt capsule, and Re-lined Pt capsule,



163 enabled us to investigate the influence of capsule materials on element loss under  
164 reducing conditions.

165 To quantitatively explore the effects of these three capsule materials, we calculated  
166 the relative loss of V, Cr, Mn, Fe, Co, Ni, Cu, Zn, Ga, Ge, Cd, In, Sn, W, and Mo in  
167 experiments E3, E4, and E5 (Supplementary Table 2). The relative loss of an element  
168 denotes the percentage of element loss relative to the starting material and is expressed as  
169 follows:

$$\text{Relative Loss} = \frac{C_{\text{STM}} - C_{\text{RP}}}{C_{\text{STM}}} \times 100 (\%),$$

170 where  $C_{\text{STM}}$  and  $C_{\text{RP}}$  are the contents of a certain element in the starting material and run  
171 products (i.e., quenched glass in this study), respectively. The relative loss can vary from  
172 0% (no element loss) to 100% (complete loss). Here, we divided the relative loss into  
173 four grades: no loss (< 10%), slight loss (10%–30%), moderate loss (30%–70%), and  
174 severe loss (> 70%).

175 In the case of the Pt capsule (E3) shown in Fig. 3a, Fe, Co, Ni, Cu, Zn, Ga, Ge, Cd,  
176 In, Sn, W, and Mo are lost severely (relative loss ~ 100%), whereas V, Cr, and Mn are lost  
177 moderately (relative loss > 50%). The different relative loss among elements should be  
178 governed by the binary metal phase diagram that defines the miscibility between two  
179 metals (Hultgren et al., 1973). In the cases of graphite-lined (E4) and Re-lined (E5) Pt  
180 capsules, all elements except Co, Ni, and Cu show slight or no loss, suggesting that the  
181 graphite and Re lining can effectively prevent element loss (Fig. 3a). The reduced relative  
182 loss for most elements in E4 indicates that they were lost to the Pt capsule in E1–E3. The

183 severe loss of Ni, Cu, and perhaps Co in E4 may be caused by diffusion through the  
184 graphite wall to alloy with the Pt capsule, or by reaction with graphite to form carbide.  
185 We also note that the concentration of W in E4 is three times higher than in the HMB  
186 glass (relative loss = -235), and infer that W contamination may have been introduced by  
187 the graphite plug on the top of the capsule (Fig. 1b). This plug was machined from a  
188 piece of graphite heater which was turned out to be W-bearing. Other parts of the graphite  
189 lining and graphite disks in other experiments were made of specpure graphite.  
190 Additionally, the Re-lined capsule performs slightly better than the graphite-lined capsule  
191 in reducing Co loss. In summary, by mechanically isolating the samples from the Pt  
192 capsule, graphite and Re can prevent the loss of V, Cr, Mn, Fe, Zn, Ga, Ge, Cd, In, Sn, W,  
193 and Mo, but do not substantially reduce the loss of Ni and Cu.

194

### 195 **The effect of experimental $fO_2$**

196 The  $fO_2$  in two experiments was buffered by loading layers of Re–ReO<sub>2</sub> or Ru–RuO<sub>2</sub>  
197 mixtures at the bottom and top of the starting materials (Fig. 1d and e), following  
198 methods outlined in Armstrong et al. (2019), Mallmann and O'Neill (2007), and Zhang et  
199 al. (2017). The redox buffers were made by mixing equal weight proportions of metal and  
200 oxides. The ratios of HMB powder to Re–ReO<sub>2</sub> buffer (E6) and Ru–RuO<sub>2</sub> buffer (E7)  
201 were 1:1 and 4:1, respectively. After the experiments, the redox buffers contain both  
202 metal and oxides, verifying the activity of the buffering reactions. At the experimental  
203 conditions investigated here, the calculated  $fO_2$  values are ~FMQ+2 for the Re–ReO<sub>2</sub>

204 buffer and ~FMQ+5 for the Ru–RuO<sub>2</sub> buffer (O'Neill and Nell, 1997; Pownceby and  
205 O'Neill, 1994). Including experiment E3, we have three samples using Pt capsules that  
206 can be used to investigate the effect of  $fO_2$  on the loss behavior of elements (i.e.,  
207 <FMQ–2, FMQ+2, and FMQ+5).

208 As shown in Fig. 3b, compared with the experiment under reducing conditions (E3;  
209  $fO_2 < \text{FMQ} - 2$ ), the loss of most elements can be prevented by elevating the experimental  
210  $fO_2$ . Only Cu, Ni, Co, In, and Sn were lost at  $fO_2$  of ~FMQ+2 (E6; Re–ReO<sub>2</sub> buffer), and  
211 only Cu exhibited moderate loss at  $fO_2$  of ~FMQ+5 (E7; Ru–RuO<sub>2</sub> buffer). We also  
212 observed an extremely high Re concentration ( $21792 \pm 1974$  ppm) in the quenched glass  
213 in E6, indicating that the dissolution of ReO<sub>2</sub> occurred. In conclusion, element loss can be  
214 prevented by elevating the experimental  $fO_2$ . The loss of V, Cr, Mn, Fe, Zn, Ga, Ge, Cd,  
215 W, and Mo can be prevented under Re–ReO<sub>2</sub> buffered conditions and all 15 elements  
216 except Cu are retained in samples under Ru–RuO<sub>2</sub> buffered conditions.

## 217 **IMPLICATIONS**

218 Experiments performed at 1.0 GPa and 1400 °C show that: (1) 15 elements,  
219 including V, Cr, Mn, Fe, Co, Ni, Cu, Zn, Ga, Ge, Cd, In, Sn, W, and Mo, are readily lost  
220 from the experimental samples by alloying with Pt capsules under reducing conditions; (2)  
221 graphite- and Re-lined capsules can prevent or substantially reduce the loss of V, Cr, Mn,  
222 Fe, Zn, Ga, Ge, Cd, In, Sn, W, and Mo, but do not prevent the loss of Ni and Cu; (3)  
223 element loss can be reduced under oxidizing conditions, and all of the elements

224 investigated here except Cu are retained in the samples under Ru–RuO<sub>2</sub> buffered  
225 conditions. These findings have several important implications. First, accurate  
226 mineral/melt partition coefficients for most elements (except for Ni and Cu) could be  
227 determined by using either graphite-lined or Re-lined capsules, or by elevating the  
228 experimental  $fO_2$ . Second, partition coefficients for Ni can be obtained under Ru–RuO<sub>2</sub>  
229 buffered conditions, while partition coefficients for Cu can only be accurately determined  
230 by using Cu-bearing alloy as the sample capsule, as demonstrated by Zajacz et al. (2011)  
231 and Liu et al. (2014, 2015). Finally, it's promising to experimentally determine melt/fluid  
232 partition coefficients for ore-forming elements by mass-balance calculations under Ru–  
233 RuO<sub>2</sub> buffered conditions.

234

235

#### ACKNOWLEDGMENTS

236 This project was financially supported by the National Key Research and Development  
237 Program of China (Grant No. 2018YFA0702704) to Xiaolin Xiong; by the Strategic  
238 Priority Research Program (XDB18000000) and President's International Fellowship  
239 Initiative (2017VSA001) of the CAS to Eiichi Takahashi. All data supporting the  
240 conclusions of this paper can be found in "<http://dx.doi.org/10.17632/5vvgf8xsgv.1>"  
241 (Mendeley Data). We greatly appreciate the constructive comments by Jon Blundy and  
242 John C. Ayers, which have improved many aspects of this work. We also thank Don  
243 Baker for the handling of this manuscript. This is contribution NO. IS-xxxx from  
244 GIGCAS.

245

246

247

## REFERENCE CITED

248 Adam, J., and Green, T. (2006) Trace element partitioning between mica- and amphibole-bearing garnet

249 lherzolite and hydrous basanitic melt: 1. Experimental results and the investigation of controls on

250 partitioning behaviour. *Contributions to Mineralogy and Petrology*, 152(1), 1-17.

251 Armstrong, K., Frost, D.J., McCammon, C.A., Rubie, D.C., and Boffa Ballaran, T. (2019) Deep magma

252 ocean formation set the oxidation state of Earth's mantle. *Science*, 365(6456), 903-906.

253 Canil, D. (1997) Vanadium partitioning and the oxidation state of Archaean komatiite magmas. *Nature*, 389,

254 842-845.

255 Davidson, J., Turner, S., Handley, H., Macpherson, C., and Dosseto, A. (2007) Amphibole “sponge” in arc

256 crust? *Geology*, 35(9), 787-790.

257 Elburg, M., Vroon, P., van der Wagt, B., and Tchalikian, A. (2005) Sr and Pb isotopic composition of five

258 USGS glasses (BHVO-2G, BIR-1G, BCR-2G, TB-1G, NKT-1G). *Chemical Geology*, 223(4),

259 196-207.

260 Fellows, S.A., and Canil, D. (2012) Experimental study of the partitioning of Cu during partial melting of

261 Earth's mantle. *Earth and Planetary Science Letters*, 337-338, 133-143.

262 Filiberto, J., Jackson, C., Le, L., and Treiman, A.H. (2009) Partitioning of Ni between olivine and an

263 iron-rich basalt: Experiments, partition models, and planetary implications. *American Mineralogist*,

264 94(2-3), 256-261.

265 Foley, S., Tiepolo, M., and Vannucci, R. (2002) Growth of early continental crust controlled by melting of

- 266 amphibolite in subduction zones. *Nature*, 417(6891), 837-840.
- 267 Grove, T.L. (1981) Use of FePt alloys to eliminate the iron loss problem in 1-atmosphere gas mixing  
268 experiments: Theoretical and practical considerations. *Contributions to Mineralogy and Petrology*,  
269 78, 298-304.
- 270 Hultgren, R., Desai, P.D., Hawkins, D.T., Gleiser, M., Kelley, K.K., and Wagman, D.D. (1973) Selected  
271 values of the thermodynamic properties of binary alloys. American Society for Metals, Metals  
272 Park, Ohio.
- 273 Kawamoto, T., and Hirose, K. (1994) Au-Pd sample containers for melting experiments on iron and water  
274 bearing systems. *European Journal of Mineralogy*, 6(3), 381-386.
- 275 Lee, C.-T.A., Leeman, W.P., Canil, D., and Li, Z.-X.A. (2005) Similar V/Sc systematics in MORB and arc  
276 basalts: Implications for the oxygen fugacities of their mantle source regions. *Journal of Petrology*,  
277 46(11), 2313-2336.
- 278 Lee, C.T.A., and Tang, M. (2020) How to make porphyry copper deposits. *Earth and Planetary Science*  
279 *Letters*, 529.
- 280 Li, L., Xiong, X.L., and Liu, X.C. (2017) Nb/Ta fractionation by amphibole in hydrous basaltic systems:  
281 Implications for arc magma evolution and continental crust formation. *Journal of Petrology*, 58(1),  
282 3-28.
- 283 Liu, X., Xiong, X., Audéat, A., and Li, Y. (2015) Partitioning of Cu between mafic minerals, Fe–Ti oxides  
284 and intermediate to felsic melts. *Geochimica et Cosmochimica Acta*, 151, 86-102.
- 285 Liu, X.C., Xiong, X.L., Audéat, A., Li, Y., Song, M.S., Li, L., Sun, W.D., and Ding, X. (2014) Partitioning  
286 of copper between olivine, orthopyroxene, clinopyroxene, spinel, garnet and silicate melts at upper

- 287 mantle conditions. *Geochimica Et Cosmochimica Acta*, 125, 1-22.
- 288 Mallmann, G., and O'Neill, H.S.C. (2007) The effect of oxygen fugacity on the partitioning of Re between  
289 crystals and silicate melt during mantle melting. *Geochimica et Cosmochimica Acta*, 71(11),  
290 2837-2857.
- 291 Matzen, A.K., Baker, M.B., Beckett, J.R., and Stolper, E.M. (2013) The temperature and pressure  
292 dependence of nickel partitioning between olivine and silicate melt. *Journal of Petrology*, 54(12),  
293 2521-2545.
- 294 Matzen, A.K., Wood, B.J., Baker, M.B., and Stolper, E.M. (2017) The roles of pyroxenite and peridotite in  
295 the mantle sources of oceanic basalts. *Nature Geoscience*, 10(7), 530-535.
- 296 Medard, E., McCammon, C.A., Barr, J.A., and Grove, T.L. (2008) Oxygen fugacity, temperature  
297 reproducibility, and H<sub>2</sub>O contents of nominally anhydrous piston-cylinder experiments using  
298 graphite capsules. *American Mineralogist*, 93(11-12), 1838-1844.
- 299 Merrill, R.B., and Wyllie, P.J. (1973) Absorption of iron by platinum capsules in high-pressure rock melting  
300 experiments. *American Mineralogist*, 58(1-2), 16-20.
- 301 O'Neill, H.S.C., and Nell, J. (1997) Gibbs free energies of formation of RuO<sub>2</sub>, IrO<sub>2</sub>, and OsO<sub>2</sub>: A  
302 high-temperature electrochemical and calorimetric study. *Geochimica et Cosmochimica Acta*,  
303 61(24), 5279-5293.
- 304 Philpotts, J.A., and Schnetzler, C.C. (1970) Phenocryst-matrix partition coefficients for K, Rb, Sr and Ba,  
305 with applications to anorthosite and basalt genesis. *Geochim Cosmochim Acta*, 34, 307-322.
- 306 Portnyagin, M.V., Mironov, N.L., and Nazarova, D.P. (2017) Copper partitioning between olivine and melt  
307 inclusions and its content in primitive island-arc magmas of kamchatka. *Petrology*, 25(4), 419-432.

- 308 Pownceby, M.I., and O'Neill, H.S.C. (1994) Thermodynamic data from redox reactions at high  
309 temperatures. IV. Calibration of the Re-ReO<sub>2</sub> oxygen buffer from EMF and NiO+Ni-Pd redox  
310 sensor measurements. *Contributions to Mineralogy and Petrology*, 118, 130-137.
- 311 Rapp, R.P., Shimizu, N., and Norman, M.D. (2003) Growth of early continental crust by partial melting of  
312 eclogite. *Nature*, 425(6958), 605-609.
- 313 Ratajeski, K., and Sisson, T.W. (1999) Loss of iron to gold capsules in rock-melting experiments. *American*  
314 *Mineralogist*, 84(10), 1521-1527.
- 315 Schnetzler, C.C., and Philpotts, J.A. (1970) Partition coefficients of rare-earth elements between igneous  
316 matrix material and rock-forming mineral phenocrysts-II. *Geochim Cosmochim Acta*, 34,  
317 331-340.
- 318 Sobolev, A.V., Hofmann, A.W., Kuzmin, D.V., Yaxley, G.M., Arndt, N.T., Chung, S.L., Danyushevsky, L.V.,  
319 Elliott, T., Frey, F.A., Garcia, M.O., Gurenko, A.A., Kamenetsky, V.S., Kerr, A.C., Krivolutsкая,  
320 N.A., Matvienkov, V.V., Nikogosian, I.K., Rocholl, A., Sigurdsson, I.A., Sushchevskaya, N.M.,  
321 and Teklay, M. (2007) The amount of recycled crust in sources of mantle-derived melts. *Science*,  
322 316(5823), 412-417.
- 323 Sobolev, A.V., Hofmann, A.W., Sobolev, S.V., and Nikogosian, I.K. (2005) An olivine-free mantle source of  
324 Hawaiian shield basalts. *Nature*, 434(7033), 590-597.
- 325 Wang, J.T., Xiong, X.L., Takahashi, E., Zhang, L., Li, L., and Liu, X.C. (2019) Oxidation state of arc  
326 mantle revealed by partitioning of V, Sc, and Ti between mantle minerals and basaltic melts.  
327 *Journal of Geophysical Research-Solid Earth*, 124(5), 4617-4638.
- 328 Xiong, X., Keppler, H., Audéat, A., Ni, H., Sun, W., and Li, Y. (2011) Partitioning of Nb and Ta between



- 329 rutile and felsic melt and the fractionation of Nb/Ta during partial melting of hydrous metabasalt.  
330 *Geochimica et Cosmochimica Acta*, 75(7), 1673-1692.
- 331 Xiong, X.L. (2006) Trace element evidence for growth of early continental crust by melting of  
332 rutile-bearing hydrous eclogite. *Geology*, 34(11), 945-948.
- 333 Xiong, X.L., Adam, J., and Green, T.H. (2005) Rutile stability and rutile/melt HFSE partitioning during  
334 partial melting of hydrous basalt: Implications for TTG genesis. *Chemical Geology*, 218(3-4),  
335 339-359.
- 336 Zajacz, Z., Candela, P.A., and Piccoli, P.M. (2017) The partitioning of Cu, Au and Mo between liquid and  
337 vapor at magmatic temperatures and its implications for the genesis of magmatic-hydrothermal ore  
338 deposits. *Geochimica et Cosmochimica Acta*, 207, 81-101.
- 339 Zajacz, Z., Candela, P.A., Piccoli, P.M., Wälle, M., and Sanchez-Valle, C. (2012) Gold and copper in  
340 volatile saturated mafic to intermediate magmas: Solubilities, partitioning, and implications for ore  
341 deposit formation. *Geochimica et Cosmochimica Acta*, 91, 140-159.
- 342 Zajacz, Z., Seo, J.H., Candela, P.A., Piccoli, P.M., and Tossell, J.A. (2011) The solubility of copper in  
343 high-temperature magmatic vapors: A quest for the significance of various chloride and sulfide  
344 complexes. *Geochimica et Cosmochimica Acta*, 75(10), 2811-2827.
- 345 Zhang, H.L., Hirschmann, M.M., Cottrell, E., and Withers, A.C. (2017) Effect of pressure on Fe<sup>3+</sup>/ΣFe  
346 ratio in a mafic magma and consequences for magma ocean redox gradients. *Geochimica et*  
347 *Cosmochimica Acta*, 204, 83-103.
- 348 Zhang, L., Ren, Z.Y., Xia, X.P., Yang, Q., Hong, L.B., and Wu, D. (2019) In situ determination of trace  
349 elements in melt inclusions using laser ablation inductively coupled plasma sector field mass

350 spectrometry. Rapid Commun Mass Spectrom, 33(4), 361-370.

351

352

### Figure Captions

353 **Figure 1.** Schematic diagrams showing the sample assemblies inside the Pt capsules (the upper row),  
354 and corresponding back-scattered electron (BSE) images of the experimental run products (the lower  
355 row). The experimental run number is marked in the top left of the BSE images. Note that in E6, the  
356 glass breaks into pieces during cutting and therefore it is not present in-situ.

357

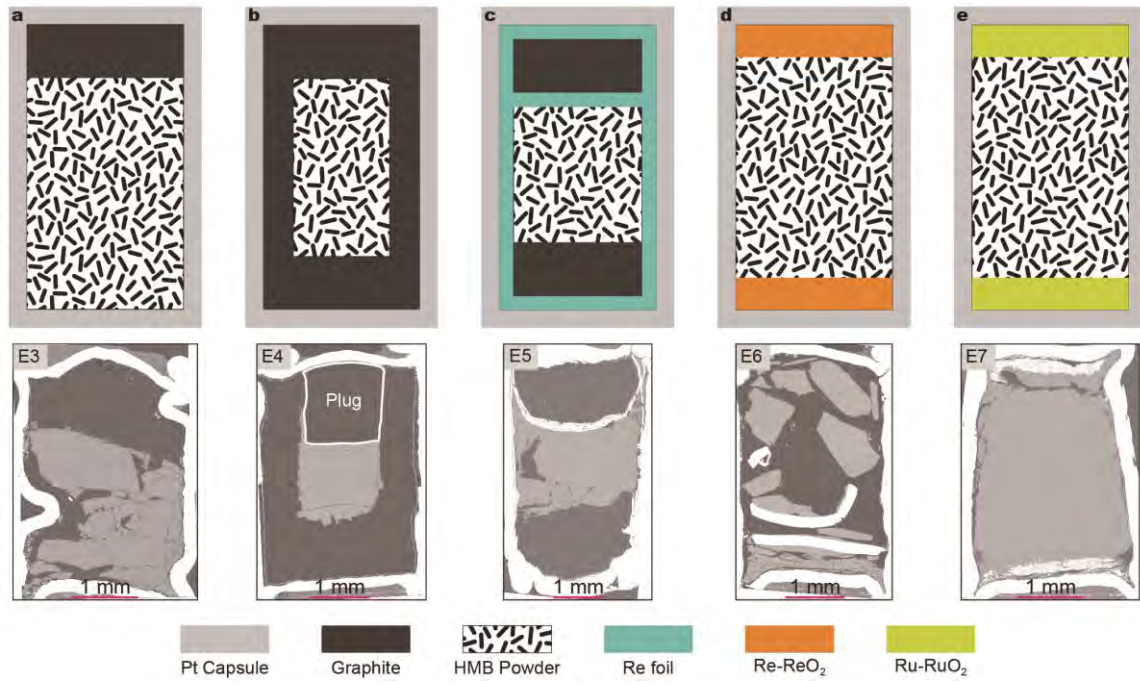
358 **Figure 2.** Results of time-series experiments performed at 1.0 GPa and 1400 °C under reducing  
359 conditions (graphite-buffered). **(a)** HMB (starting material)-normalized element concentrations in the  
360 experimental run products. The sample/HMB concentration ratios for 15 elements (V, Cr, Mn, Fe, Co,  
361 Ni, Cu, Zn, Ga, Ge, Cd, In, Sn, W, and Mo) are <1.0, indicating loss of those elements during the  
362 experiments. No loss was observed for other elements, including Si, Al, Mg, Ca, Na, K, P, Sc, Ti, Li, B,  
363 Rb, Sr, Ba, Cs, La, Ce, Pr, Nd, Sm, Eu, Gd, Ho, Yb, Lu, Y, Zr, Hf, Nb, and Ta. **(b)** Changes in the  
364 concentrations of the 15 elements with experimental duration, which demonstrated that 22 h is  
365 sufficient for diffusional equilibrium at the utilized experimental conditions. The 0 h sample represents  
366 the starting material.

367

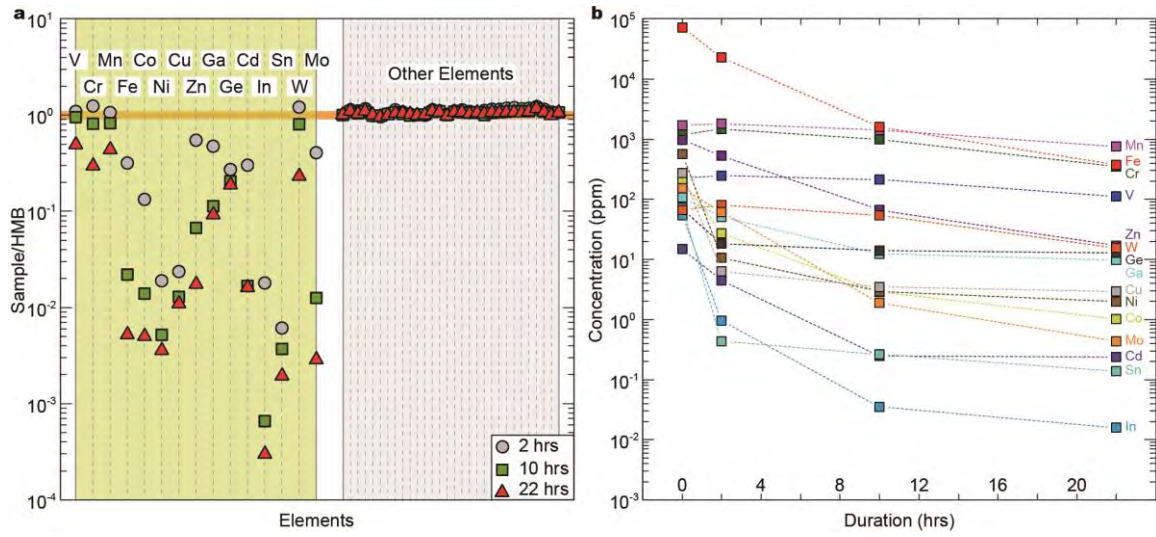
368 **Figure 3.** The effects of capsule material and experimental  $fO_2$  on the mobility of elements. **(a)** The  
369 effect of capsule material on the relative loss of elements under reducing condition (graphite-buffered).  
370 In the case of the Pt capsule (E3), the relative loss of the 15 elements is higher than 50 wt.%, and Fe,

371 Co, Ni, Cu, Zn, Cd, In, Sn, and Mo were almost lost completely. In the cases of graphite-lined (E4)  
372 and Re-lined (E5) Pt capsules, only Cu, Ni, and Co were severely lost. Note that there was W  
373 contamination in E4 due to the graphite plug containing a high concentration of W, resulting in the  
374 negative relative loss of W in this experiment. The shaded brown area denotes the region of no  
375 element loss in this study (<10%). **(b)** The effect of experimental  $fO_2$  on the relative loss of elements  
376 in Pt capsule experiments. Most of the 15 elements are lost under reducing conditions (E3;  
377 graphite-buffered). This can be prevented by elevating the experimental  $fO_2$ : only Cu, Ni, Co, In, and  
378 Sn were lost at  $fO_2$  of ~FMQ+2 (E6: Re–ReO<sub>2</sub> buffer), and only Cu was lost at  $fO_2$  of ~FMQ+5 (E7:  
379 Ru–RuO<sub>2</sub> buffer).

380 **Figure 1**

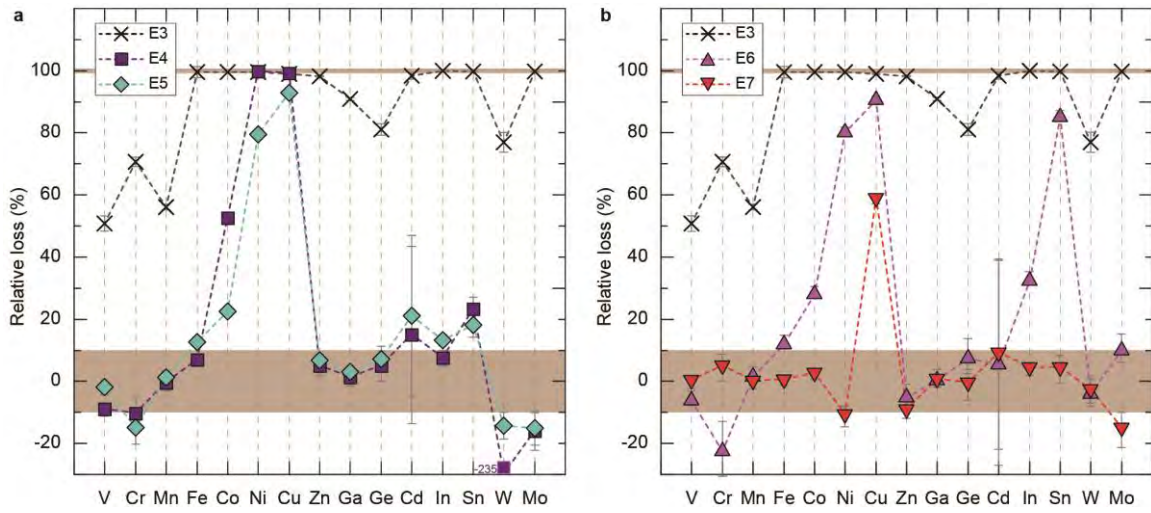


382 **Figure 2**



383

384 **Figure 3**



385

386

387